Physico-Chemical Interaction between Mineral Admixtures and OPC-Calcium Sulfoaluminate (CSA) Cements and its Influence on Early-age Expansion

Piyush Chaunsali[1] and Paramita Mondal[2*]

[1]Graduate Student, Department of Civil and Environmental Engineering, University of Illinois, Urbana, IL 61801, USA, Email: chaunsa2@illinois.edu

[2*]Corresponding Author, Assistant Professor, Department of Civil and Environmental Engineering, University of Illinois, Urbana, IL 61801, USA, Email: pmondal@illinois.edu

Abstract

The present study aims at examining the physico-chemical factors influencing the expansion characteristics of OPC-CSA blend in the presence of mineral admixtures. Three different admixtures: Class 'F' fly ash ('F'FA), Class 'C' fly ash ('C'FA) and silica fume (SF) were used as 15%, 15% and 5% replacement of total cementitious binder. Longitudinal expansion of cement pastes prepared at w/cm – 0.44 showed that the Class 'F'FA increased the expansion whereas the Class 'C'FA and SF reduced the expansion. The pore solution of the OPC-CSA cement pastes was extracted at different ages to monitor the concentration of various ionic species. The saturation level of ettringite was determined using a geochemical modeling program (GEMS). Furthermore, an upper bound of crystallization stress was estimated. The expansion behavior in the presence of Class 'F'FA and SF was found to be influenced by the changes in the stiffness, whereas the expansion of the Class 'C'FA-based mixture was governed by faster hydration of ye'elimite.

Keywords: Calcium sulfoaluminate cement (D); Early-age expansion (C); X-ray diffraction (B); Supersaturation (C); Crystallization (C); Ettringite (D); Thermodynamic modeling (B)

1. Introduction

Calcium sulfoaluminate (CSA) cements were originally developed and promoted as shrinkage-compensating cements [1]. Different combinations of CSA cements with ordinary Portland cement (OPC) have been used for various structural applications [2]. In structural concrete, the presence of restraint can fully or partially prevent the expansion of OPC-CSA concrete, which leads to the development of compressive stress that can be utilized to counteract the tensile stress developed due to drying shrinkage. Recently, there has been a tremendous increase in the research of CSA cements as its manufacturing is supposed to be more sustainable than that of the Portland cement. CSA clinkers can be produced at lower kiln temperature (~1250°C) which reduces energy consumption considerably [3-6]. The limestone requirement is lower for producing CSA clinkers, which reduces the associated CO_2 emission. Additionally, CSA clinkers require less energy for grinding as they are more porous than the Portland cement clinker [7, 8]. These factors contribute toward reducing the energy demand and carbon footprint of CSA cements. Ye'elimite ($C_4A_3\hat{S}$) is the main phase present in CSA cements along with other phases such as belite (C_2S), calcium sulfate ($C\hat{S}$) and ferrite (C_4AF) in CaO-Al_2O_3-SiO_2-Fe_2O_3-SO_3 system [7, 8]. Based on the amount of added gypsum, various kinds of cements, ranging from rapid-hardening to expansive, can be produced [9]. The main hydration reactions associated with ye'elimite hydration are shown below [10]:

$$C_4A_3\hat{S} + 18H \rightarrow C_3A.C\hat{S}.12H + 2AH_3 \quad (1)$$

$$C_4A_3\hat{S} + 2C\hat{S}H_2 + 34H \rightarrow C_3A.3C\hat{S}.32H + 2AH_3 \quad (2)$$

$$C_4A_3\hat{S} + 6CH + 8C\hat{S}H_2 + 74H \rightarrow 3C_3A.3C\hat{S}.32H + 2AH_3 \quad (3)$$

where C = CaO, A = Al_2O_3, S = SiO_2, $\hat{S}$ = SO_3, H = H_2O according to the cement chemistry notation. According to reaction (1), it is evident that the hydration of ye'elimite in pure water forms AFm (monosulfate) and amorphous aluminum hydroxide. When there is sufficient sulfate in form of gypsum or anhydrite, ettringite (AFt) will be formed instead of monosulfate, according to reaction (2) [8, 11]. However, a few studies have reported the formation of ettringite even in the absence of a sulfate source [12, 13]. Furthermore, reaction (3) is favored over reaction (2) in presence of portlandite. An increase in portlandite amount has been found to increase the rate of ye'elimite hydration at very early-age and decrease the induction period [14].

According to Mehta [15], presence of portlandite results in the precipitation of smaller ettringite crystals which tend to be expansive due to their swelling characteristics. Among various proposed mechanisms of expansion, crystallization stress theory is a widely accepted mechanism according to which crystals grow from a supersaturated solution [16-18]. The upper bound of crystallization pressure, as set by supersaturation, can be expressed as [19]:

$$\sigma_C = \frac{RT}{\nu_m} \ln\left(\frac{K}{K_{sp}}\right) \quad \text{Eq. (1)}$$

where R, T, ν_m, K and K_{sp} are ideal gas constant (8.314 J/K/mol), absolute temperature (°K), molar volume, ion activity product and solubility product of a given crystal, respectively. Supersaturation governs the size of pores where crystals can precipitate [17]. For example, smaller crystals have higher surface energy which increases their solubility. Therefore, smaller crystals can only achieve equilibrium with a solution of higher concentration. Hence, supersaturation can be related to the pore sizes where precipitation of crystal occurs according to Freundlich equation [20]:

$$\gamma_{CL}\kappa_{CL} = \frac{RT}{\nu_m} \ln\left(\frac{K}{K_{sp}}\right) \quad \text{Eq. (2)}$$

where γ_{CL} and κ_{CL} are the interfacial free energy and the curvature of crystal, respectively. The expression shows that crystals will precipitate in pores with higher curvature (i.e. smaller pore size) if the supersaturation is high. In fact, in a related study on delayed ettringite formation (DEF), it has been argued that the initial expansion takes place due to crystallization in nanometric pores under high supersaturation [18].

Understanding the expansion characteristics of CSA cements is important for achieving shrinkage-compensation successfully. A number of factors have been shown to affect the early-age expansion behavior of CSA cements including the degree of hydration of $C_4A_3\hat{S}$ [21], $C\hat{S}/C_4A_3\hat{S}$ ratio [22, 23], presence of lime [15, 24-27], particle size distribution of CSA cements [23, 28], curing condition [29] and curing temperature [21]. As CSA cements can expand significantly on its own, the expansion can be controlled by blending it with the Portland cement. A blend of CSA cement and the Portland cement (OPC-CSA blend) is also called Type K cement [30]. In an OPC-CSA blend with low CSA cement content (less than 30%), hydration of

ye'elimite occurs in the presence of lime (free lime and portlandite) and forms ettringite [31]. In a study by Le Saoût et al., a 10% CSA cement addition to OPC was reported not to affect the hydration mechanism of alite but retarded the C_3A reaction due to the presence of sulfates, and increased the amount of ettringite [32]. In a study by Mehta [15], ettringite was reported to have smaller size in the presence of lime, whereas Kurdoski and Thiel [25] did not observe any difference in the ettringite morphology.

Incorporating mineral admixtures with CSA cements is expected to have some economic and environmental benefits. Additionally, the use of mineral admixtures such as fly ash is expected to result in improved workability, reduced heat of hydration, higher ultimate strength and increased chemical resistance [33-35]. However, there have been very few studies toward understanding the expansion potential of Type K cement (OPC-CSA blend) in the presence of mineral admixtures and insufficient research is limiting practical application [36, 37]. Lobo and Cohen [36] reported a decrease in expansion of Type K cement incorporating silica fume which was attributed to reduced pH of pore solution resulting in a slower reaction rate of ye'elimite. In a recent study by García-Maté et al. [33], no evidence of the interaction between fly ash and CSA cement hydration was found. This study examines the early-age unrestrained expansion of OPC-CSA cements in the presence of two types of fly ashes (Class 'C' and 'F') and silica fume. To better understand the influence of these admixtures while preventing the dilution of CSA cement, a fixed quantity of expansive component (15% by weight of total cementitious material) was used in this study. Physical changes, such as evolution of stiffness with time, and chemical changes, such as concentration of various ionic species in pore fluid, supersaturation levels of various phases such as ettringite and portlandite, and hydration of ye'elimite were monitored to understand the expansion characteristics. Furthermore, crystallization stresses in OPC-CSA cements were estimated using various models. It is believed that better understanding of expansion behavior in the presence of mineral admixtures is warranted as it can help the end user in making better predictions.

2. Materials and Mixture Proportions

The materials used in this study were a Type I ordinary Portland cement (OPC), a CSA-based expansive admixture manufactured by CTS company (trade name Komponent), Class 'C' fly ash ('C'FA), Class 'F' fly ash ('F'FA) and silica fume (SF). Table 1 shows the oxide composition of

all raw materials. The phase composition of raw materials was determined using quantitative X-ray diffraction (QXRD) analysis, and is shown in Table 2.

Table 1. Chemical composition of raw materials

	OPC	Komponent	'F' FA	'C' FA	SF
SiO_2	20.93	7.70	59.08	37.76	> 93.0
Al_2O_3	4.45	7.00	22.43	19.43	--
Fe_2O_3	2.72	1.17	8.39	5.33	--
CaO	63.28	50.07	1.59	25.56	--
MgO	3.03	0.08	1.06	4.09	--
SO_3	2.44	26.04	0.20	2.23	--
Na_2O	0.13	0.18	0.64	1.07	--
K_2O	0.59	0.53	2.18	--	--
LOI	1.98	2.10	2.99	0.58	<6%

Table 2. Phase composition (% wt.) of raw materials by QXRD

Phase Composition	OPC	Komponent	Class 'F' FA	Class 'C' FA
C_3S	62.2	--	--	--
C_2S	14.1	35.0	--	--
C_3A	9.9	--	--	7.0
C_4AF	5.4	1.5	--	--
Ye'elimite	--	19.4	--	--
Gypsum	1.4	14.7	--	--
Bassanite	1.6	9.4	--	--
Anhydrite	0.8	16.3	--	1.3
Quartz	--	--	15.8	3.2
Mullite	--	--	21.3	--
Hematite	--	--	0.8	0.2
Periclase	1.3	0.9	--	1.0
Arcanite	0.4	--	--	--
Aphthitalite	0.1	--	--	--
Calcite	2.8	2.8	--	--
Amorphous	--	--	62.2	87.3

Total	100	100	100	100

Cement paste samples were prepared with a constant water-to-cementitious material ratio (w/cm) of 0.44 at 22°C. A portion of the Portland cement was replaced by the CSA-based expansive admixture (Komponent) and one of the mineral admixtures ('C'FA or 'F'FA or SF). Komponent, Class 'C'FA, Class 'F'FA, and SF were used as 15%, 15%, 15% and 5% replacement (by mass) of the total cementitious material, respectively. Therefore, five different mixtures: 1) 100% Portland cement (OPC), 2) 85% Portland cement and 15% Komponent (OPC+K), 3) 70% Portland cement, 15% Komponent, and 15% Class 'C'FA (OPC+K+'C'FA), 4) 70% Portland cement, 15% Komponent, 15% Class 'F'FA (OPC+K+'F'FA), and 5) 80% Portland cement, 15% Komponent, and 5% silica fume (OPC+K+SF) were examined in this study.

3. Experimental Methods

3.1. Unrestrained Deformation at Early-age

As the primary goal of this study was to examine the early-age expansion characteristics, it was important to select a test method which allows length measurements at the early-age (within 24 hours). Considering the fact that ettringite starts forming immediately after mixing, but does not contribute to the stress build-up until a certain degree of rigidity is reached by the cement matrix [38], final setting time was chosen as the starting point for the expansion measurements. Final setting of cement pastes was determined using a Vicat needle apparatus in accordance to ASTM C191. Though primarily intended for determining autogenous shrinkage of cement paste, the corrugated tube test method, as per the ASTM C1698, was selected for expansion measurement in this study. The method is equally appropriate as the length measurements in the longitudinal direction can be made due to the least resistance offered by the corrugated tube in this direction. Also, the measurements can be started immediately after encapsulating paste in a corrugated tube. It is noted here that corrugated tube maintains a sealed curing condition inside the tube, and hence, were only used for measuring expansion occurring within the first 24 hours.

In addition to the corrugated tube test, prismatic bars of size 1 in (25 mm) × 1 in (25 mm) × 11.25 in (285 mm) were prepared to determine the effects of lime water curing on the expansion measurements. Samples were demolded after 24 hours, and kept in saturated lime water at 22°C. The length changes were monitored at various ages according to the ASTM C490. Three samples

were prepared for each batch at two different times. The standard deviation of the length measurements was found to be within ±5%. The initial expansion measured through corrugated tube (within the first 24 hours) was added to the length measurements of prismatic samples (beyond 24 hours) to estimate the total expansion from the final set time.

3.2. X-ray Diffraction (XRD)

Mineralogical composition of the basic materials and the evolution of hydrated phases were monitored using XRD. At each age, samples of 2-3 mm thickness were immersed in isopropyl alcohol for 24 hours in order to stop the hydration. Subsequently, the samples were dried in a vacuum desiccator for at least 24 hours. It has been shown that most of the methods used for stopping hydration dehydrate C-S-H and ettringite to some extent [39]. However, the results should be comparable if the same preparation method is followed throughout the study. The dried samples were then ground into a fine powder (< 40μm) for XRD analysis. Initially, qualitative analysis was performed using the MDI Jade software (2009) in order to identify crystalline phases. Once all phases were identified, the HighScore Plus (Version 3.0e) software was used for Rietveld analysis [40], which relies on the minimization of the differences between the measured and the calculated pattern, using a non-linear least squares fitting algorithm. The refined parameters included phase scale factors, background coefficients, zero-shift error, lattice parameters, peak shape parameters and preferred orientation, if needed. An internal standard method based on the addition of rutile (TiO_2) was utilized to determine the amorphous content of basic materials and of the hydrated cement paste [41]. Rutile was found to be appropriate as an internal standard as there was no trace of it in CSA-based admixture (Komponent). Rutile was ground with the dried cement paste samples after solvent exchange.

3.3. Thermogravimetric (TG) Analysis

Thermogravimetric analysis was performed on 25 ± 2 mg of the powdered (prepared following the method described in section 3.2) samples using a Q50-TA Instrument. The samples were heated in a nitrogen environment (flow: 60 ml/min) to 900°C at a rate of 10°C per minute.

3.4. Pore Solution Analysis and Thermodynamic Modeling

Cement paste samples of 2 in (50 mm) in diameter × 3 in (75 mm) in height were used for pore solution extraction. Samples were prepared using de-ionized (DI) water at a w/cm ratio of 0.44.

These samples underwent a similar curing regime (24 hours of sealed curing followed by saturated lime water curing) as used for the prismatic samples. The pore solution was extracted after 1, 3, 7, and 21 days. A device proposed by Barneyback and Diamond [42] was used for the extraction. The samples were compressed to a pressure up to 400 MPa in order to extract 5-10 ml of the pore solution. It is noted here that the applied stress has been found to influence the ionic concentrations in the pore solution [43]. However, the ionic concentrations in the pore solution extracted by applying pressure up to approximately 500 MPa, have been found to be comparable [44]. In this study, the applied maximum pressure ranged from 300 MPa to 400 MPa, depending on the age of the sample. Immediately after extraction, the pore solution was filtered using a 0.2 µm filter. One part of the extracted pore solution was treated with 6.3% HNO_3 to prevent carbonation, and was later used for the determination of Ca, Al, Si, S, Na and K element concentrations, using Inductively Coupled Plasma Optical Emission Spectrometry (ICP-OES). The rest of the pore solution was used for pH measurement. A pH meter was calibrated against known KOH solutions for determining hydroxyl ion concentration.

Using the aqueous phase composition of the cement pore solution, the hydration process can be monitored by estimating the saturation index (SI) of the possible reaction products in contact with the aqueous phase. The saturation index can be expressed as [45, 46]:

$$SI = \ln\left(\frac{K}{K_{sp}}\right) \qquad \text{Eq. (3)}$$

where K is the ion activity product and K_{sp} is the solubility product of a given phase. If SI = 0, the solution is at equilibrium, whereas for SI > 0 and SI < 0, the solution is supersaturated and undersaturated with respect to a given crystal, respectively. The dissolution reaction of ettringite can be expressed in the following form [44-45]:

$$Ca_6Al_2(SO_4)_3(OH)_{12}.26H_2O \leftrightarrow 6Ca^{2+} + 2Al(OH)_4^- + 3SO_4^{2-} + 4OH^- + 26H_2O \qquad \text{Eq. (4)}$$

Now, considering the ionic species forming ettringite, the ion activity product of ettringite can be written as:

$$K(ettringite) = \{Ca^{2+}\}^6 \{Al(OH)_4^-\}^2 \{OH^-\}^4 \{SO_4^{2-}\}^3 \{H_2O\}^{26} \qquad \text{Eq. (5)}$$

where $\{Ca^{2+}\}$, $\{Al(OH)_4^-\}$, $\{OH^-\}$, $\{SO_4^{2-}\}$ and $\{H_2O\}$ are the activities of species. The solubility product (K_{sp}) of ettringite at 25°C is $10^{-44.90}$ [47, 48]. The activity of an ion is the product of ion concentration (m_i), and activity coefficient (γ_i). The activity coefficient, which depends on ionic strength of the solution (I), other ionic species and temperature, can be calculated using extended Debye-Hückel equation as [49]:

$$\log \gamma_i = \frac{-Az_i^2\sqrt{I}}{1+Ba_i\sqrt{I}} + b_i I \qquad \text{Eq. (6)}$$

where A and B are Debye- Hückel solvent parameters and dependent only on temperature, a_i is the Debye-Hückel ion-size parameter, b_i is a semi-empirical parameter (~ 0.064 at 25°C), z_i is the charge of ion and I is the effective ionic strength ($I = ½\sum m_i z_i^2$ in mol/kg H_2O) of the solution. Using ion activity product and solubility product of a phase, its saturation level in the pore solution can be determined using Eq. (3). When the aqueous phase is supersaturated with respect to a specific solid (i.e., SI >0), there is tendency for precipitation of the solid until equilibrium is reached. Similarly, in an undersaturated condition (SI < 0), the solid will tend to dissolve in order to achieve equilibrium. In this study, the thermodynamic calculations to estimate saturation indices were performed by using a geochemical modeling package: GEMS-PSI [50, 51] which was supplemented with cement specific thermodynamic database [52].

3.5. Capillary Porosity

Capillary porosity of the cement paste samples was determined by the solvent exchange method [53]. Cement paste disks of 25 mm (diameter) × 1-2 mm (thickness) were cut and immersed in isopropyl alcohol for 24 hours. Afterward, the volume of the samples was determined by the buoyancy method using isopropyl alcohol as the liquid medium. Subsequently, the samples were dried in a vacuum desiccator. The weight difference due to drying was attributed to the removal of capillary water. Finally, capillary porosity was calculated by dividing capillary pore volume by the sample volume.

3.6. Dynamic Modulus Test

Stiffness of cement paste samples of 1.5 in (38 mm) × 1.5 in (38 mm) × 6 in (150 mm) was monitored by performing a dynamic modulus test according to the ASTM C215. The longitudinal resonant frequency was measured to calculate the dynamic elastic modulus (E) of the paste samples according to the following relationship:

230 $$Dynamic\ E\ (in\ pascals) = D\ M\ n^2 \quad \text{Eq. (7)}$$

231 where D = 4 L /(b × t) for a prismatic sample of size *b* (in meters) × *t* (in meters) × *L* (in meters),
232 *M* is the mass of the sample (in kg), and *n* is the fundamental longitudinal frequency (in Hz).

233 # 4. Results and Discussion

234 ## 4.1. Unrestrained Expansion

235 Figure 1 (a) shows the expansion characteristics of the OPC and the OPC-CSA cement paste.
236 The addition of the CSA-based admixture increased the expansion significantly. The expansion
237 occurring within 24 hours was significant, which suggests the importance of starting the
238 expansion measurement at the final set [54]. It is evident that most of the expansion was
239 complete in the first 7 days. Although the OPC-CSA cement paste exhibited an expansion of
240 ~0.6% (6000 με), it did not show any visible cracking. Furthermore, structural integrity of the
241 samples was verified by monitoring the dynamic modulus, which did not show any drop in
242 modulus values during the period when expansion occurred (data presented in a later section). In
243 a recent study by the authors [55], cracking in the OPC-CSA blends was not observed until a
244 higher (30%) CSA cement content was used. Excessive cracking was also reflected by the
245 reduction in the dynamic modulus [55]. The difference in expansion potential of the OPC and the
246 OPC-CSA paste is mainly due to formation of abundant ettringite crystals in the OPC-CSA
247 paste. Expansion characteristics were also monitored for the sample containing Class 'C'FA,
248 Class 'F'FA and SF and are shown in Fig. 1 (b). The Class 'F'FA resulted in the highest
249 expansion, whereas Class 'C'FA reduced the expansion of the OPC-CSA cement pastes. Unlike
250 other samples, the OPC-CSA cement paste with Class 'C'FA ceased expanding beyond 2 days as
251 evident from Fig. 1 (b). It is noted here that the maximum expansion in this study was ~ 0.7%
252 (7000 με) and no visible cracking was observed in those samples. In a study by Chen et al. [23],
253 CSA cement pastes showing ~1% expansion did not exhibit cracking either, however, samples
254 with ~5% expansion did. In order to explain the expansion characteristics, ye'elimite hydration,
255 ettringite content, crystallization stress and material stiffness were monitored and are discussed
256 in subsequent sections.

257

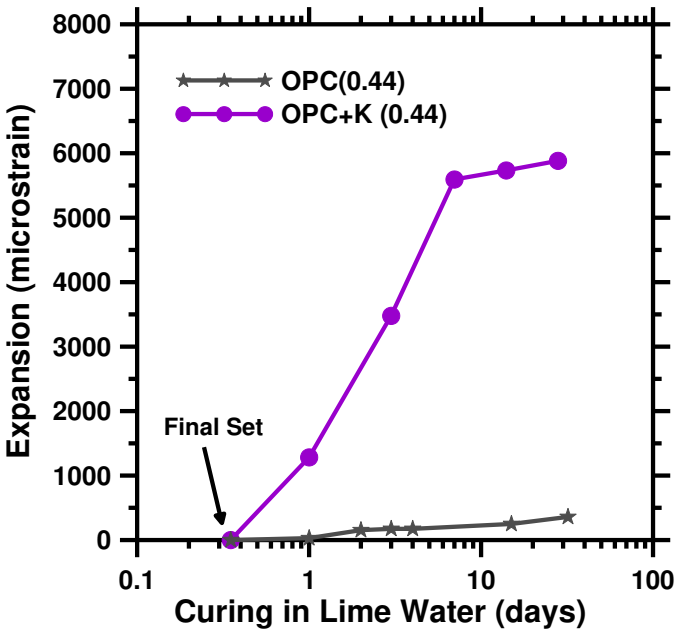

(a)

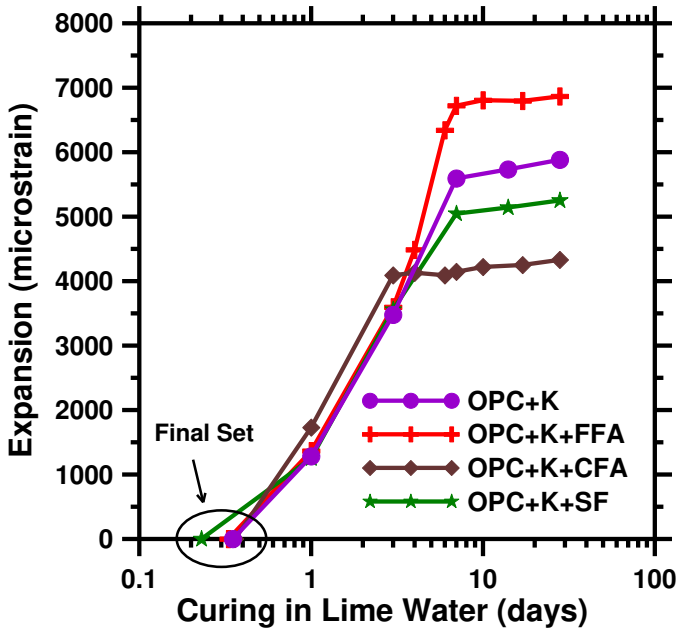

(b)

Figure 1. Unrestrained expansion of: (a) OPC and OPC-CSA cement pastes, and (b) OPC-CSA cement pastes in presence of mineral admixtures under saturated lime water curing at w/cm – 0.44

4.2. Hydration of Ye'elimite and Evolution of Ettringite

The progress of ye'elimite hydration was monitored using X-ray diffraction coupled with Rietveld analysis. Table 3 shows the phase compositions of CSA-based pastes at various ages: 0, 1, 3 and 7 days. The data presented in Table 3 represents the values obtained from Rietveld refinement on samples after solvent exchange without accounting for the chemical bound water. A clear difference in the amount of ettringite is evident between the plain OPC and all OPC-CSA pastes. The hydration of ye'elimite in OPC-CSA pastes results in the formation of additional ettringite compared to the plain OPC paste. The quantitative XRD analysis indicates that the most of the ettringite in the OPC-CSA paste samples was formed within the first 24 hours, after which there was only small or no further increase. The ettringite content in all OPC-CSA pastes seemed to be comparable. Therefore, the increased ettringite content in the OPC-CSA pastes explained higher expansion in those samples compared to the plain OPC paste. However, the difference in expansion of the OPC-CSA pastes with various mineral admixtures had no strong correlation with the ettringite content. The lack of strong correlation between the ettringite content and the expansion characteristics was also reported in previous studies [56, 57]. As mentioned previously, samples with the Class 'C'FA achieved the maximum expansion in 2 days whereas the expansion process lasted for 6-8 days for the other mixtures (Fig. 1 (b)). XRD analysis (Fig. 2) confirmed faster reaction of ye'elimite in the Class 'C'FA mixture as ye'elimite could not be detected in Class 'C'FA mixture after 3 days, which explains the early completion of the expansion process. Chaunsali and Mondal [58] showed that the C_3A content of Class 'C'FA resulted in early depletion of gypsum which was evident by the presence of a shoulder in calorimetry curve. The early depletion of gypsum promoted the formation of AFm phases in Class 'C'FA mixtures as evident in Fig. 2. It should be noted here that strätlingite could not be detected in the cement pastes examined in this study.

294 Table 3. Evolution of hydrated phases (% weight) in CSA-based cement pastes using Rietveld X-
295 ray diffraction analysis (accuracy within ± 2%). Last column reports portlandite (CH) content
296 from thermogravimetric analysis.

Phase	Age	C_3S	C_2S	C_3A	C_4AF	$C_4A_3\hat{S}$	Ett.	CH	Amor.	CH(TG)
OPC	0	62.2	14.1	9.9	5.4	0.0	0.0	0.0	0.0	0.0
	1	22.9	14.4	1.8	1.9	0.0	5.0	10.8	39.9	9.0
	3	13.3	12.5	0.8	1.2	0.0	2.9	15.5	48.5	14.2
	7	8.6	14.8	0.3	1.1	0.0	1.5	18.2	51.6	16.0
OPC+K	0	52.9	17.2	8.4	4.9	2.9	0.0	0.0	0.0	0.0
	1	16.3	13.7	7.4	1.9	1.1	10.7	8.9	35.9	7.7
	3	10.0	14.6	1.3	1.5	0.4	10.4	11.4	47.9	10.0
	7	11.8	12.5	0.1	0.6	0.1	10.0	12.8	49.0	12.0
OPC+K+FFA	0	43.5	15.1	6.9	4.1	2.9	0.0	0.0	0.0	0.0
	1	10.6	10.7	5.8	1.4	1.2	9.2	6.5	49.8	6.0
	3	9.4	10.7	1.4	1.3	0.3	10.2	9.8	49.8	9.1
	7	5.7	8.5	0.2	0.7	0.0	9.2	9.3	60.5	9.9
OPC+K+CFA	0	43.5	15.1	8.0	4.1	2.9	0.0	0.0	0.0	0.0
	1	14.8	11.1	5.9	1.2	1.1	10.2	4.5	46.8	4.8
	3	6.8	10.9	0.9	0.9	0.0	7.9	7.0	63.3	6.6
	7	3.2	12.0	0.6	0.8	0.0	7.6	7.3	65.0	9.3
OPC+K+SF	0	49.8	16.5	7.9	4.6	2.9	0.0	0.0	0.0	0.0
	1	12.5	11.5	6.0	1.0	1.1	8.5	9.4	47.9	6.3
	3	8.3	12.3	1.8	1.6	0.6	11.2	10.2	51.1	8.2
	7	6.9	12.3	0.7	1.2	0.0	10.7	10.0	55.7	10.0

297 Amor. – C-S-H and AFm

298 CH (% wt. from TG) = $\frac{W_{380^oC} - W_{420^oC}}{W_{30^oC}} \times \frac{MW_{CH}}{MW_{H_2O}} \times 100$

299 where $MW_{CH} = 74$ and $MW_{H2O} = 18$

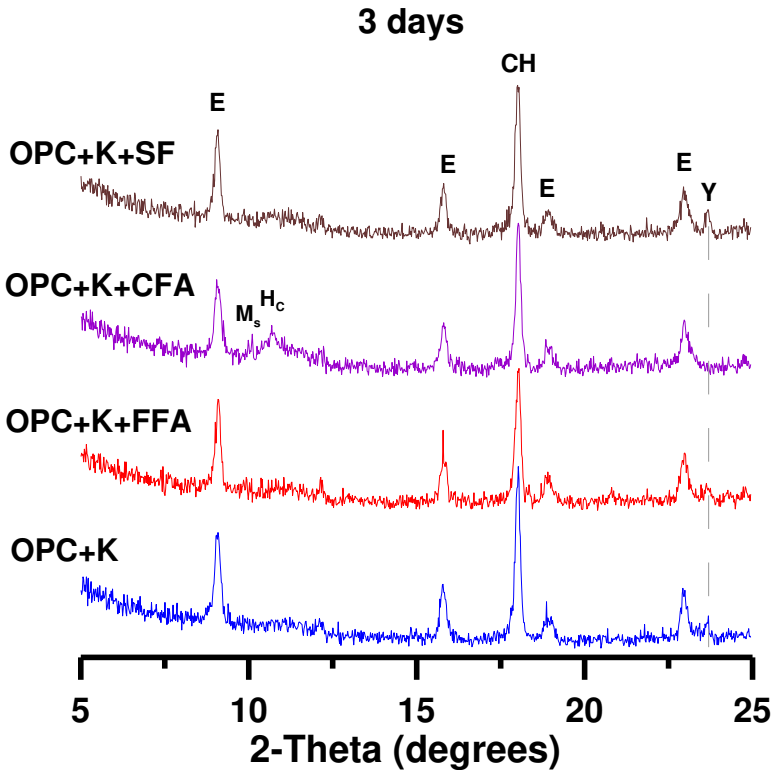

Figure 2. X-ray diffraction patterns of OPC-CSA cement pastes at the age of 3 days (Note: E – ettringite, CH – portlandite, Y – ye'elimite, M_s – monosulfate, H_c –hemicarbonate)

Thermogravimetric (TG) analysis of OPC-CSA cement samples is presented in Fig. 3. The weight loss of all samples between 30-800°C was 15-17% (of initial weight) after 1 day of hydration, and increased to 20-25% (of initial weight) after 7 days of hydration. This increase in weight-loss mainly resulted from the dehydration of hydration products such as C-S-H (e.g. in the X-ray amorphous fraction), portlandite and AFm phases. Derivative thermogravimetric (DTG) analysis, showed the presence of ettringite, portlandite and calcite peaks in all samples. Furthermore, AFm peak was evident in the plain OPC (at both 1 and 7 days) and OPC+K+'C'FA mixture (at 7 days) due to early depletion of gypsum. No peak corresponding to gibbsite (AH_3) was observed in any of the samples. As evident from the DTG analysis, the peak corresponding to the dehydration of ettringite showed significant overlap for all OPC-CSA cement pastes with mineral admixtures. This indicates that the amounts of ettringite formation in those mixtures are comparable. The observation matches with the QXRD data presented previously. This confirms that the insignificant difference in the ettringite content among OPC-CSA cement samples cannot explain the significant difference in their expansion characteristics. The amount of

317 portlandite as calculated from TG analysis was found to be in good agreement with the values
318 obtained from QXRD.

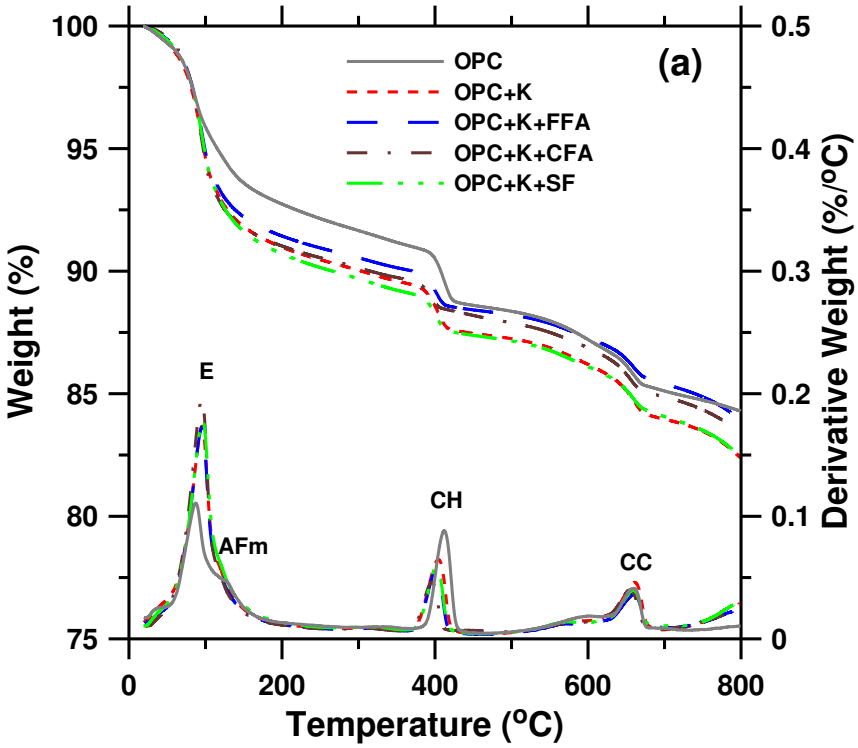

319

320

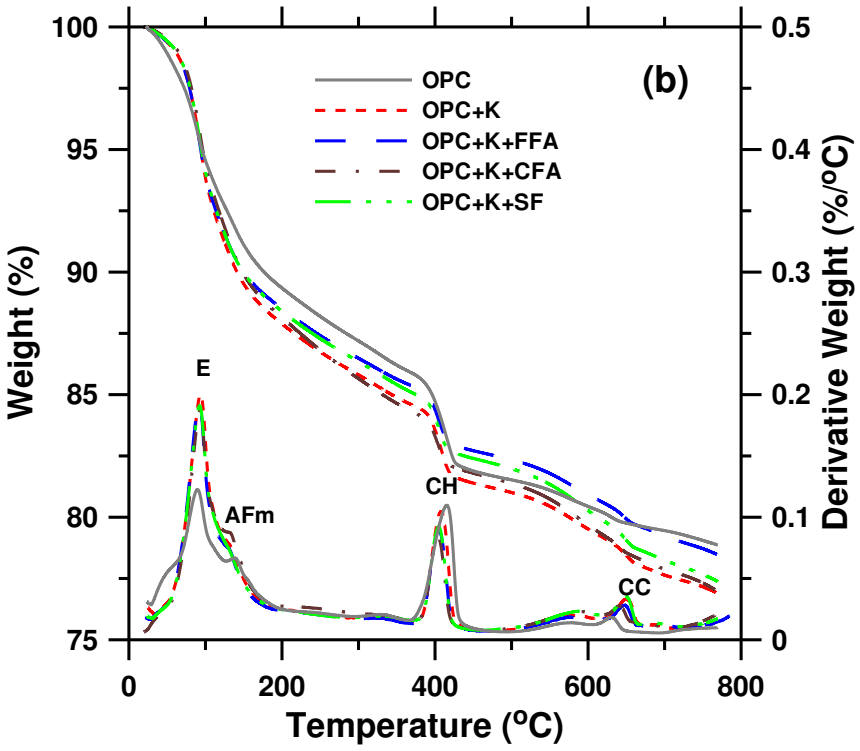

Figure 3. Thermogravimetric (TG) and derivative thermogravimetric (DTG) analysis of OPC and CSA-based cement paste after: a) 1 day, and b) 7 days

4.3. Pore Solution Chemistry and Degree of Supersaturation

The crystallization stress depends on supersaturation with respect to a crystal, the volume of crystals exerting pressure, microstructure and the locations where the crystals are formed. From thermodynamics, the maximum crystallization stress can be evaluated using saturation index with respect to the crystal in pore solution according to Eq. (1). Therefore, at first, the elemental compositions of Ca, Si, Al, S, Na and K in pore solution were measured using ICP-OES analysis. The variation in Na, K, Ca and S element concentrations were within ±20% between replicates. Figure 4 presents the evolution of the concentrations of various elements in the pore solution of OPC and OPC-CSA cement pastes. Overall, the concentration of various elements was found to be in general agreement with available data from literature on CSA cements [59, 60]. The Ca concentration decreased beyond 1 day due to the precipitation of ettringite, portlandite, and C-S-H. Aluminum and silica concentrations in the pore solution were found to be lower than 1 mM at all times. The formation of ettringite resulted in a decrease in S concentration with time by consuming the sulfates from the pore solution. As expected, the S concentration in the OPC paste was found to be lower than in the OPC-CSA pastes (Fig. 4). The pH of the OPC-CSA system

was found to be in the range of 12.6-13.1. As reported in previous studies, the pH of the OPC-CSA cement system was found to be lower than that of the OPC system [59, 60]. Alkali concentration in the pore solution increased from 1 day to 7 days due to continuous release of alkalis during the dissolution of anhydrous phases causing an increase in pH. The pore solution pH of OPC+K+'F'FA and OPC+K+SF cement pastes was lower than the OPC+K cement paste. It has been suggested that C-S-H with a low Ca/Si ratio formed due to a pozzolanic reaction tends to adsorb the alkalis, especially K^+ ions [43, 61] lowering the alkali concentration. Here, the pozzolanic reaction refers to the reaction between portlandite (from C_3S and C_2S hydration) and glassy fraction of fly ash and silica fume. Among all mixtures, the pH of SF paste was found to be the lowest at the end of 21 days, suggesting the alkali-binding. Additionally, the portlandite content of pastes with mineral admixtures was lower than OPC+K cement paste, which could be potentially due to the pozzolanic reaction and the dilution of OPC. The effect of the Class 'C'FA on alkali concentration of the pore solution was less pronounced than that of the Class 'F'FA, which agrees with the findings by Shehata et al.[62].

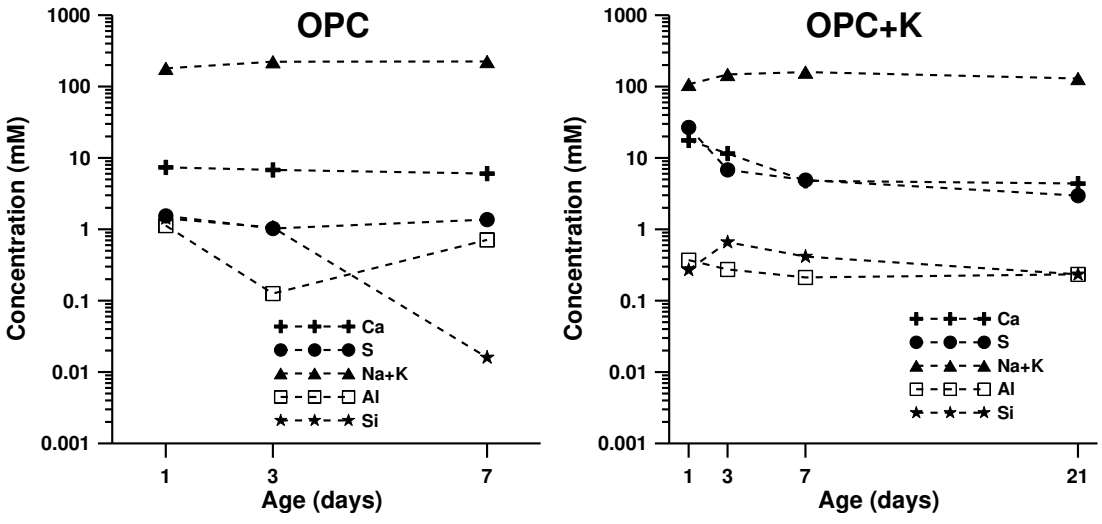

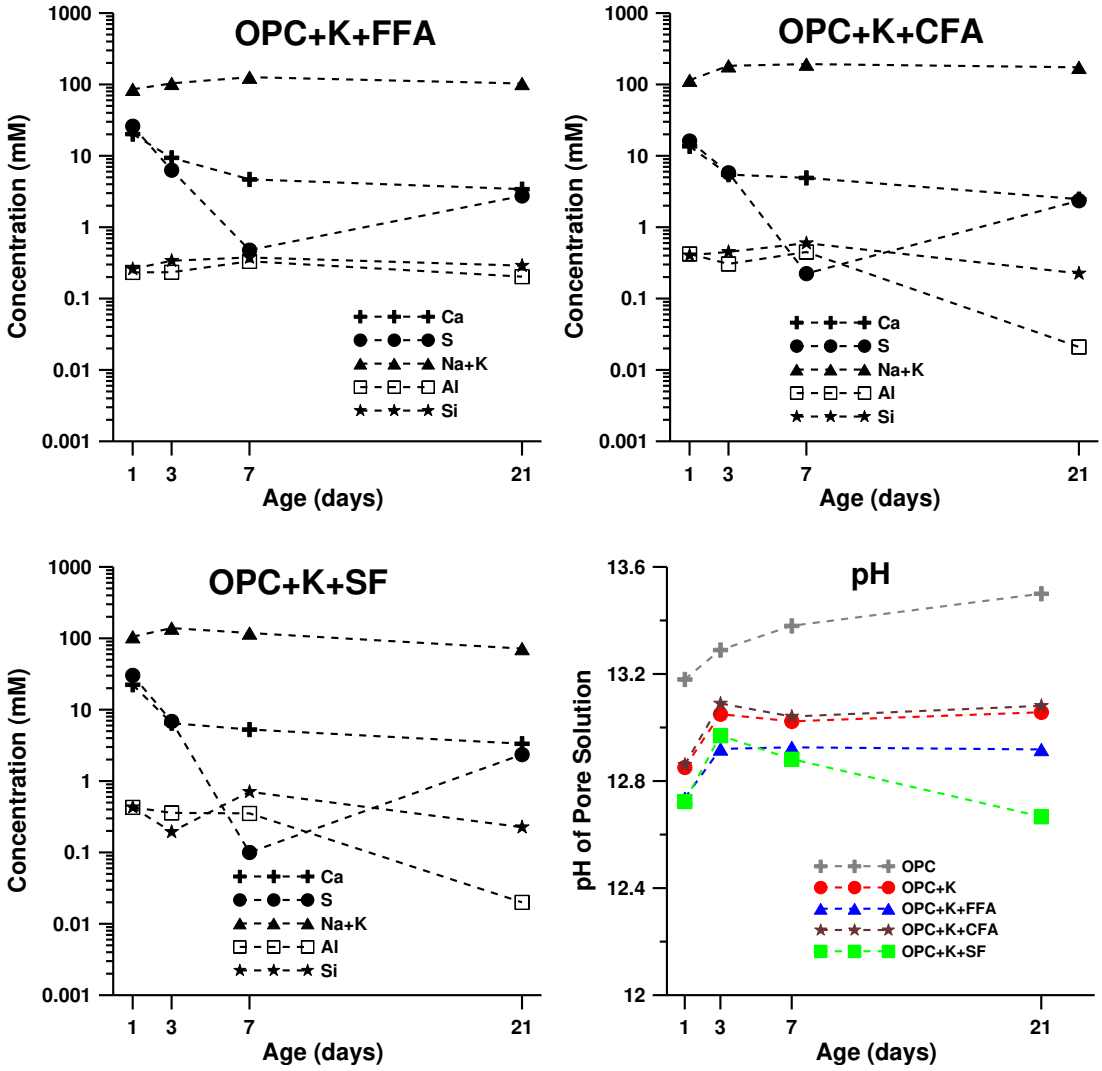

Figure 4. Elemental composition of the pore solution of OPC and OPC-CSA binders, and evolution of the pH at various ages

Figure 5 shows the saturation index (SI) of ettringite and portlandite for the OPC and the OPC-CSA cement pastes at 1, 3, 7 and 21 days. The elemental concentrations of Ca, Na, K, S, Al and Si were used as an input for calculating saturation indices using GEMS-PSI. The saturation index with respect to ettringite was higher for all OPC-CSA cement pastes compared to the OPC reference after 1 day (Fig. 5 (a)), emphasizing the importance of the sulfate concentration on the saturation and as a result, the influence of supersaturation on expansion [63]. The incorporation of mineral admixtures did not seem to result in any significant difference in SI of ettringite at 1

day; however, SI of ettringite was reduced in the presence of mineral admixture at later ages. The supersaturation with respect to ettringite in OPC-CSA cement pastes decreased with time until 7 days and did not change much thereafter. Similar SI values at 7 and 21 days indicated that there was no change in crystallization pressure from 7 to 21 days, which is supported by expansion characteristics shown in Fig. 1 (b). The portlandite appeared to be oversaturated until 7 days as shown in Fig. 5 (b).

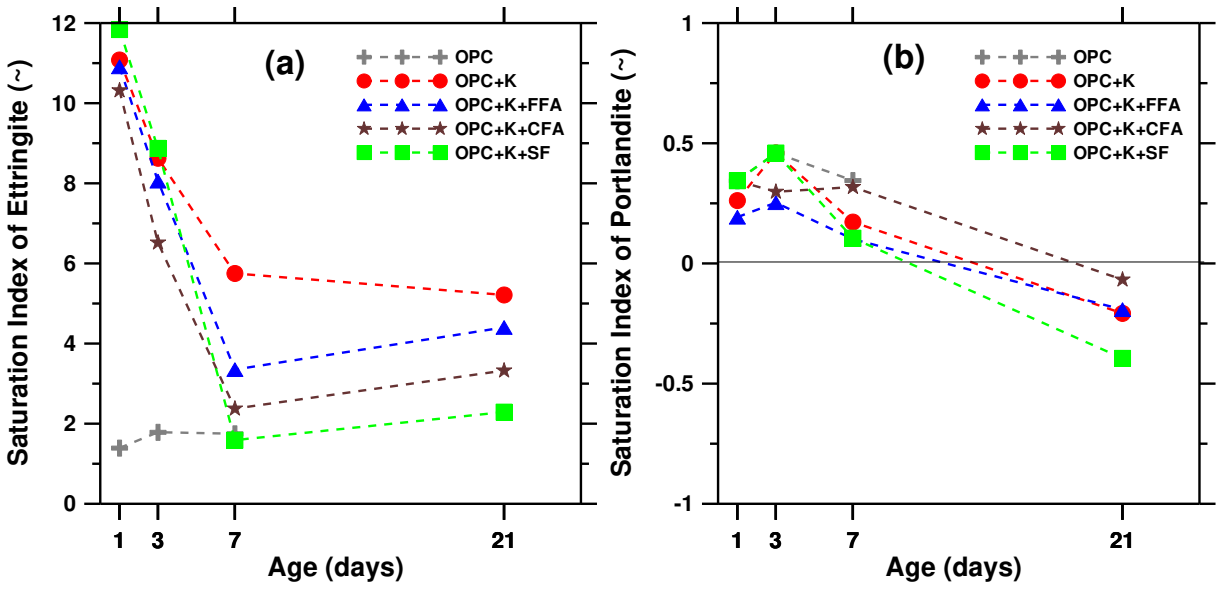

Figure 5. Saturation index of: a) ettringite and b) portlandite as a function of specimen age using measured pore solution concentration

4.4. Crystallization Stress

Crystallization stress (σ_c), which is derived from supersaturation, can be calculated using Correns's formula as described in Eq. (1). Now the average hydrostatic stress (σ) can be related to the maximum crystallization stress (σ_c) using the following expression [18]:

$$\sigma = \sigma_C f(\phi_C) \qquad \text{Eq. (8)}$$

where ϕ_c is the volume fraction of crystals exerting pressure and $f(\phi_C)$ is the geometric factor which would depend on the type of pores such as cylindrical or spherical. The average

hydrostatic tensile stress on a cylinder or sphere under an internal pressure of σ_c can be calculated as [64]:

Cylindrical pores: $$\sigma = \sigma_C \left(\frac{2\phi_C}{3 - 3\phi_C} \right) \quad \text{Eq. (9)}$$

Spherical pores: $$\sigma = \sigma_C \left(\frac{\phi_C}{1 - \phi_C} \right) \quad \text{Eq. (10)}$$

As the volume fraction of ettringite exerting pressure (ϕ_c) is expected to be lower than the total volume fraction of the ettringite crystals, the upper bound of the crystallization stress can be estimated by considering the total volume fraction of ettringite. The model described above is simplistic, and therefore, a model based on poromechanics was also utilized to estimate the crystallization stress. According to Coussy [65], at saturation and constant temperature, local crystallization pressure, σ_c, can be related to the macroscopic stress, σ, using following expression:

$$\sigma = bS_C\sigma_C \quad \text{Eq. (11)}$$

where b is the Biot coefficient and S_c is the volume fraction of crystals in total pore volume. The Biot coefficient, b can be expressed as:

$$b = 1 - \frac{K}{K_s} \quad \text{Eq. (12)}$$

where K and K_s are the bulk modulus of the porous and the solid matrix respectively. For calculating the crystallization stress, the Biot coefficient (b) was assumed 0.6 for cement paste [66]. It is noted that the constant value of b was assumed as the first approximation, although the Biot coefficient will change due to continuous evolution of K and K_s of the cement matrix. Previously, the model based on poromechanics [Eq. (11)] has been applied to investigate the salt damage in stone [67, 65]. It is evident that the volume fraction of ettringite is required for all models described above. As the Rietveld analysis provides the weight fraction of different phases in the cementitious matrix, it was necessary to convert the weight fraction into volume fraction while considering the pore volume. To accomplish this, at first, total pore volume (capillary

409 porosity) was determined using the solvent exchange method, as described in Sec. 3.5. Figure 6
410 shows the evolution of capillary porosity with time. Clearly, the Class 'F'FA-based mixture
411 showed the highest porosity at all ages and the SF-based mixture resulted in the lowest porosity
412 at the end of 7 days, possibly due to the pozzolanic reaction and pore refinement.

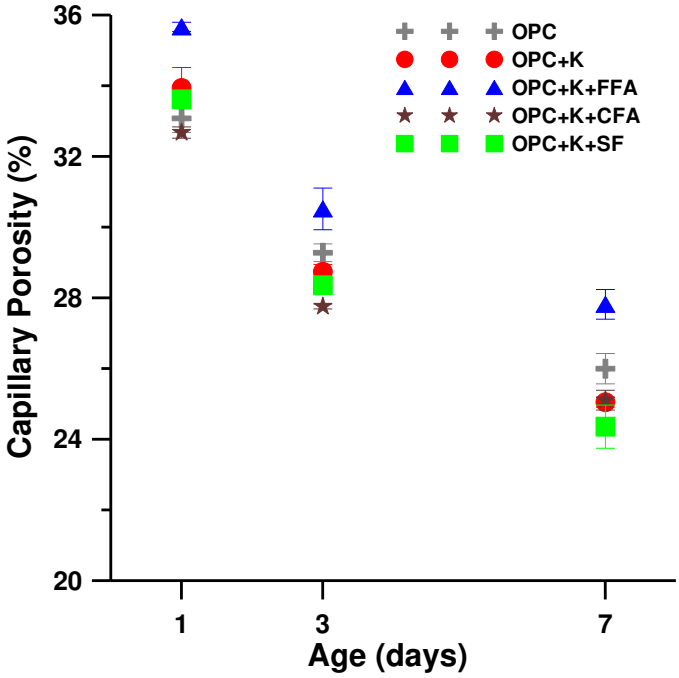

413

414 Figure 6. Evolution of capillary porosity in presence of mineral admixtures

415 Now, using the densities of various phases [69] such as ettringite, portlandite, calcite, C-S-H,
416 C_3S, C_2S, C_3A, C_4AF and $C_4A_3\hat{S}$ and total pore volume, the volume fraction of ettringite was
417 calculated. The upper bound of crystallization stress was estimated considering the total volume
418 fraction of ettringite as determined through Rietveld analysis. The curvature effects prominent
419 for crystals growing in smaller pore sizes (less than 100 nm) were not considered here [70].
420 Figure 7 shows the upper bound of crystallization stress and the evolution of tensile strength in
421 OPC-CSA cement pastes at 1, 3 and 7 days. The maximum hydrostatic tensile stress was
422 calculated using Eqs. (9), (10) and (11). The tensile stress was found to be decreasing over time,
423 being the maximum at 1 day. All tensile stresses were found to be less than 4 MPa. Fig. 7
424 compares the predicted tensile stresses due to crystallization with the measured tensile strengths
425 of all mixtures and can be used to predict tensile failure. Although, the tensile stresses of the
426 OPC-CSA pastes are higher than the corresponding measured tensile strengths at the age of 1

day, no tensile failure (cracking) was observed. This could be due to early-age tensile creep which would reduce the actual stress levels in the samples compared to the predicted values based on elastic analysis. Also, the stress calculation assumes the contribution of all ettringite as determined by QXRD; but the actual amount of ettringite exerting the stress would be lower. Therefore, it is not unreasonable to have the actual tensile stresses comparable or lower than the tensile strengths at 1 day. At the age of 3 days, the tensile stresses due to crystallization were comparable to the measured tensile strengths for all samples. The stress calculations corroborate the fact that the samples did not exhibit any cracking. The differences in crystallization stresses between the OPC and the OPC-CSA pastes are evident from Fig. 7. All three models were able to predict the higher crystallization stresses in the CSA-based cement pastes and explained the observed differences in the expansion behavior (Fig. 1). Considering the small differences in the amount of ettringite among various mixtures and similar saturation indices at early-age, the crystallization stresses does not seem to be significantly different in the OPC-CSA cement pastes with various mineral admixtures, especially at 1 day. It is noted that the difference in the pore size distribution can introduce some variation in the calculated crystallization stresses which was not considered in this study.

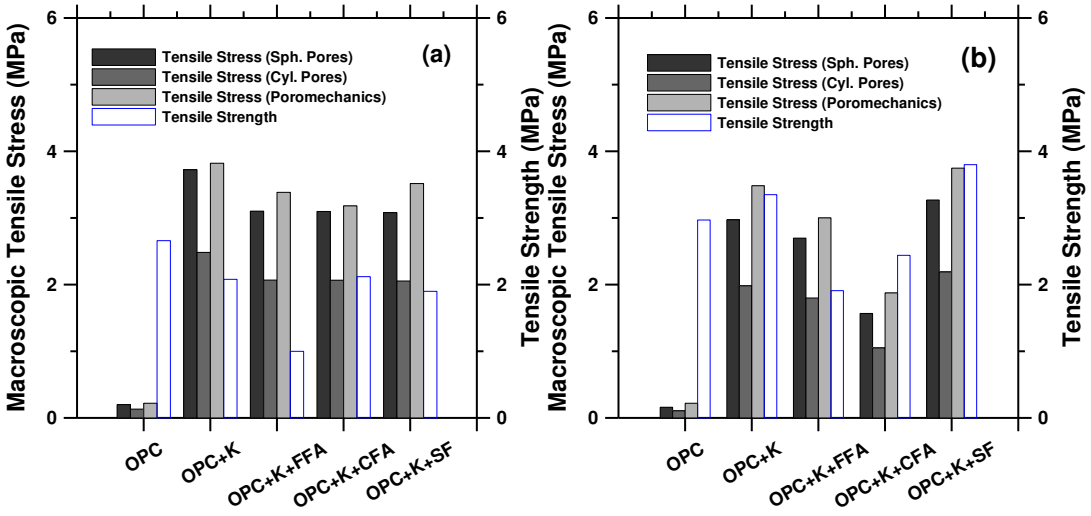

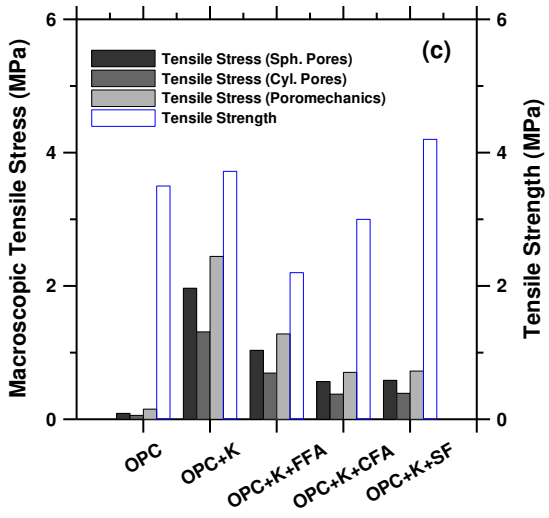

445

446 Figure 7. Macroscopic tensile stress predicted by three models vs. tensile strength at the age of:
447 a) 1 day, b) 3 days, and c) 7 days

448 **4.5. Physical Changes: Monitoring Dynamic Modulus**

449 The calculation of crystallization stresses in various OPC-CSA cement pastes did not completely
450 explain the differences in the expansion behavior, although the differences between the OPC and
451 the OPC-CSA pastes were quite evident. The behavior of the Class 'C'FA mixture was
452 predominantly influenced by the faster consumption of ye'elimite, which led to early completion
453 of the expansion process as shown in Fig. 1 (b). In order to fully explain the expansion behavior
454 of Class 'F'FA and SF mixture, the evolution of dynamic modulus (or stiffness) was monitored.
455 The deformation against an applied stress depends on the material stiffness, which means a
456 material with higher stiffness would show a lower deformation. Figure 8 shows the longitudinal
457 dynamic elastic modulus of the OPC and the OPC-CSA cement pastes. No drop in the dynamic
458 modulus of the OPC-CSA cement pastes was observed over the duration of the testing which
459 suggests the structural integrity of samples and supports the results of visual inspection. At 3
460 days, all samples except the Class 'F'FA mixture exhibited modulus values within 1%. As
461 reported earlier (Fig. 1(b)), the expansion characteristics of OPC-CSA cement pastes were
462 comparable up to 3 days. It is possibly due to the high porosity (hence low stiffness) of all the
463 OPC-CSA cement pastes at early age (up to 3 days). The deviation in expansion characteristics
464 begins in between 3 days and 7 days and the mixtures attained most of the expansion by the end
465 of 7 days. Samples with Class 'F'FA consistently showed the lowest modulus, which means it
466 offered the least resistance against crystallization stress among all mixtures, and expanded the

most. Samples with silica fume showed the highest modulus at the end of 7 days, indicating the maximum resistance against expansion. Hence, the modulus test suggests that the expansion would be lower for the SF mixture and higher for the fly ash mixtures when the crystallization stress is similar among them. Therefore, the evolution of dynamic modulus provides an insight on expansion characteristics of Class 'F'FA and SF mixtures, which could not be explained solely based on evolution of ettringite content and rate of ye'elimite hydration. Additionally, the evolution of microstructural features such as pore size distribution will influence the expansion characteristics [27].

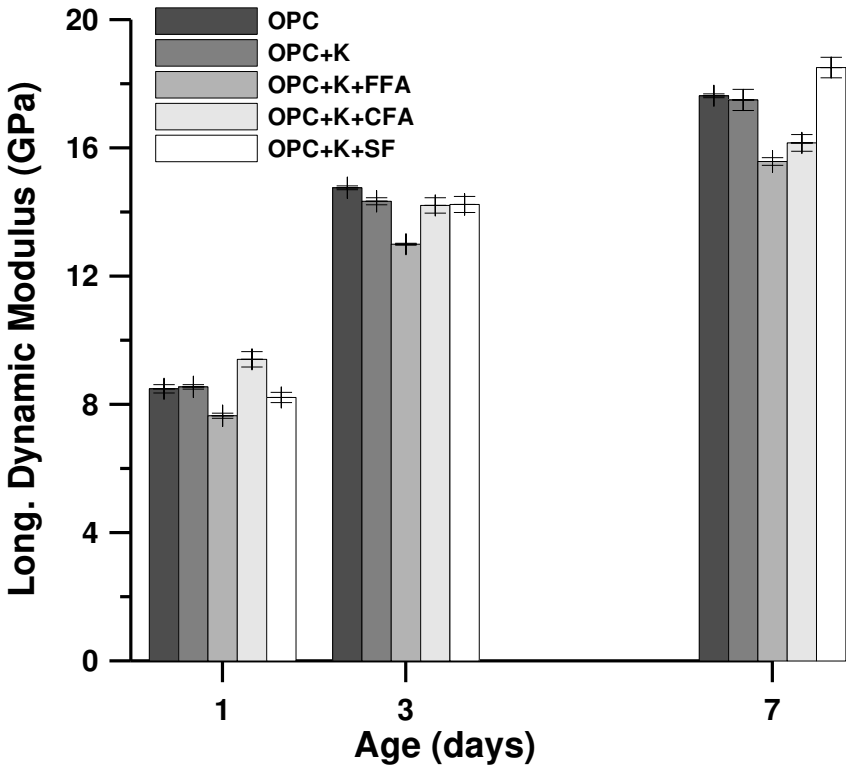

Figure 8. Longitudinal dynamic modulus of OPC and OPC-CSA pastes (Error bars represent the standard deviation of three measurements)

4.6. Comparison between Measured and Calculated Strain

In order to compare the measured strain with the calculated strain, a simple elastic approach was undertaken to calculate the strain due to crystallization stress under the assumption of isotropic and homogenous material. The longitudinal strain can be related to the crystallization stress, σ_c, according to the following equation [71]:

$$\varepsilon = \frac{\sigma_c}{3}\left(\frac{1}{K} - \frac{1}{K_s}\right) \qquad \text{Eq. (13)}$$

The bulk modulus (K) was calculated from the measured dynamic modulus (E) and assumed Poisson's ratio of 0.2 for isotropic and homogenous matrix using the relation: $K=E/3(1-2v)$, and K_s was assumed to be 48 GPa [72]. Figure 9 compares the measured strains with the calculated strain from 1 day through 7 days for CSA-based mixtures. It is evident that the observed strains are 3-4 times larger than the calculated elastic strains. One reason for such mismatch could be due to the assumption made in the calculation that the strain due to crystallization is elastic. The influence of tensile creep is expected to be high at the early age [73]. As evident from the Fig. 9, the trend of calculated expansion for the Class 'C'FA mixture matched reasonably well with the observed expansion. Furthermore, both the calculated and the measured strains for the Class 'C'FA mixture were lower than that of the other mixtures. Although the observed expansion was similar for all mixtures till 3 days, the calculated expansion of the OPC+K, OPC+K+'F'FA and OPC+K+SF mixtures were higher than that of the Class 'C'FA mixture. Additionally, there was not much increase in expansion of the mixtures beyond 3 days based on the elastic strain calculation, however, the measured expansion was observed to increase until 7 days.

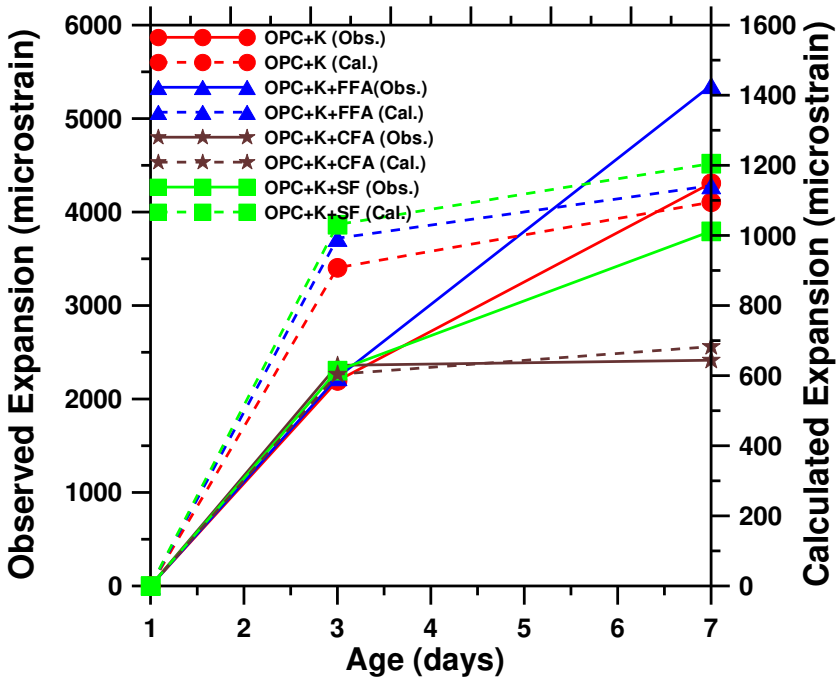

501

502 Figure 9. Comparison between experimental and calculated elastic strain for various OPC-CSA
503 mixtures (bold and dashed lines represent experimental and calculated strains, respectively)

504 After monitoring the physical and chemical changes in the OPC-CSA cement pastes, it appears
505 that the modulus values of respective paste governed the expansion characteristics during 3-7
506 day period, especially for Class 'F'FA and SF paste. The Class 'C'FA paste ceased expanding
507 earlier than other mixtures due to faster consumption of ye'elimite, hence mainly governed by
508 chemical changes. Therefore, both physical and chemical changes should be monitored to fully
509 understand the expansion characteristics in CSA-based system. Furthermore, the evolution of
510 tensile creep and pore structure features in the presence of Class 'F'FA, Class 'C'FA and SF are
511 also expected to influence the expansion characteristics.

512 ## 5. Conclusions

513 In this study, OPC-CSA cement pastes were examined in the presence of mineral admixtures and
514 the physico-chemical factors influencing expansion characteristics were studied. The following
515 conclusions can be drawn from this study:

- All mixtures with CSA cement showed much higher expansion compared to the OPC mixture. The mixture with Class 'F'FA exhibited the highest expansion among all mixtures, and the Class 'C'FA mixture ceased expanding earlier than other mixtures.
- Higher supersaturation levels of ettringite in the OPC-CSA cement pastes than the OPC paste gave rise to crystallization stress, leading to increased expansion.
- The crystallization stress in all the OPC-CSA pastes was found to be much higher than the OPC paste at 1 day. The crystallization stress started decreasing with time and did not change much after 7 days.
- The crystallization stress at 1 day was found to be similar among all the OPC-CSA cement pastes when the pore refinement, due to addition of mineral admixtures, is not considered.
- The expansion characteristics of Class 'F'FA and SF mixtures could be explained by monitoring the evolution of elastic modulus, whereas the faster consumption of ye'elimite appeared to have influenced the expansion of Class 'C'FA mixture.
- The measured strains were found to be 3-4 times larger than the calculated strains based on the elastic strain prediction from the crystallization stresses, indicating the effect of early-age creep (tensile).

Acknowledgements

The authors gratefully acknowledge the financial support provided by Illinois Center for Transportation and Illinois Department of Transportation to conduct part of this research. This study was carried out in part in the Frederick Seitz Materials Research Laboratory Central Facilities, University of Illinois. The assistance of Haiyang Zhao (previous undergraduate student at the University of Illinois) and Jeevaka Somaratna (previous graduate student at the University of Illinois) in conducting some of the experiments is highly appreciated. The authors would also like to acknowledge the insightful discussions with Prof. George W. Scherer of Princeton University and Dr. Jeffrey W. Bullard of National Institute of Standards and Technology (NIST), Gaithersburg, MD, USA.

References

[1] A. Klein, C. Troxell, Studies of calcium sulfoaluminate admixtures for expansive cements, Proc. ASTM. 58 (1958) 986-1008.

[2] G. L. Kalousek, Development of expansive cements, *Klein Symposium on Expansive Cement Concretes*. ACI Sp. Pub.38 (1973) 1-19.

[3] M.M. Ali, S. Gopal, S.K. Handoo, Studies on the formation kinetics of calcium sulphoaluminate, Cem. Concr. Res. 24 (1994) 715-720.

[4] P. Mehta, Investigations on energy-saving cements, *World Cement Technology*. 11 (1980) 166-177.

[5] G. Valenti, L. Santoro, R. Garofano, High-temperature synthesis of calcium sulphoaluminate from phosphogypsum, *Thermochim. Acta*. 113 (1987) 269-275.

[6] S. Sahu, J. Havlica, V. Tomková, J. Majling, Hydration behaviour of sulphoaluminate belite cement in the presence of various calcium sulphates, *Thermochim. Acta*. 175 (1991) 45-52.

[7] J. H. Sharp, C. D. Lawrence, R. Yang, Calcium sulfolauminate cements – low-energy cements, special cements or what?, *Adv. Cem. Res.* 11 (1999) 3-13.

[8] F. Glasser, L. Zhang, High-performance cement matrices based on calcium sulfoaluminate–belite compositions, Cem. Concr. Res. 31 (2001) 1881-1886.

[9] L. Zhang, Microstructure and Performance of Calcium Sulfoaluminate Cements, PhD Thesis. University of Aberdeen (2001). P.K. Mehta, Mechanism of expansion associated with ettringite formation, Cem. Concr. Res. 3 (1973) 1-6.

[10] M. Collepardi, R. Turriziani, A. Marcialis, Paste hydration of $4CaO.3Al_2O_3.SO_3$ in presence of calcium sulphate, tricalcium silicate and dicalcium silicate, Cem. Concr. Res. 2 (1972) 213-223.

[11] P. K. Mehta, A. Klein, Investigations on the Hydration Products in System $4CaO.3Al_2O_3.SO_3$-$CaSO_4$-CaO-H_2O, Special Report-National Research Council. Highway Research Board. (1966) 328-352.

571 [12] F. Winnefeld, S. Barlag, Calorimetric and Thermogravimetric Study on the Influence of
572 Calcium Sulfate on the Hydration of Ye'elimite, J. Therm. Anal. Cal. 3 (2010) 949-957.

573 [13] A. Cuesta, G. Álvarez-Pinazo, S.G. Sanfélix, I. Peral, M. A. G. Aranda, A. G. De la
574 Torre, Hydration Mechanisms of Two Polymorphs of Synthetic Ye'elimite, Cem. Concr. Res. 63
575 (2014) 127-136.

576 [14] C. W. Hargis, A. P. Kirchheim, P. J. M. Monteiro, E. M. Gartner, Early Age Hydration of
577 Calcium Sulfoaluminate (synthetic ye'elimite, $C_4A_3\hat{S}$) in the presence of gypsum and varying
578 amounts of calcium hydroxide, Cem. Concr. Res. 48 (2013) 105-115.

579 [15] P.K. Mehta, Mechanism of expansion associated with ettringite formation, Cem. Concr.
580 Res. 3 (1973) 1-6.

581 [16] X. Ping, J. J. Beaudoin, Mechanism of Sulphate Expansion I. Thermodynamic Principle
582 of Crystallization Pressure, Cem. Concr. Res. 22 (1992) 631–640.

583 [17] G.W. Scherer, Stress from crystallization of salt, Cem. Concr. Res. 34 (2004) 1613-1624.

584 [18] R.J. Flatt, G.W. Scherer, Thermodynamics of crystallization stresses in DEF, Cem.
585 Concr. Res. 38 (2008) 325-336.

586 [19] C.W. Correns, Growth and dissolution of crystals under linear pressure, Discuss. Faraday
587 Soc. 5 (1949) 267-271.

588 [20] H. Freundlich, Colloid and Chemistry, Methuen London, 1926.

589 [21] M. Ish-Shalom, A. Bentur, Properties of type K expansive cement of pure components I.
590 Hydration of unrestrained paste of expansive component—Results, Cem. Concr. Res. 4 (1974)
591 519-532.

592 [22] T. Desbois, R. Le Roy, A. Pavoine, G. Platret, A. Feraille, A. Alaoui, Effect of gypsum
593 content on sulfoaluminate mortars stability, Eur. J. Environ. Civ. Eng. 14 (2010) 579-597.

594 [23] I.A. Chen, C.W. Hargis, M.C.G. Juenger, Understanding expansion in calcium
595 sulfoaluminate-belite cements, Cem. Concr. Res. 42 (2012) 51-60.

596 [24] P.K. Mehta, F. Hu, Further evidence for expansion of ettringite by water adsorption, J.
597 Am. Ceram. Soc. 61 (1978) 179-181.

598 [25] W. Kurdowski, A. Thiel, On the role of free calcium oxide in expansive cements, Cem.
599 Concr. Res. 11 (1981) 29-40.

600 [26] M. Bianchi, F. Canonico, L. Capelli, M.L. Pace, A. Telesca, G.L. Valenti, Hydration
601 properties of calcium sulfoaluminate-portland cement blends, ACI SP (2009) 187-200.

602 [27] D. Gastaldi, F. Canonico, L. Capelli, L. Bianchi, M. Pace, A. Telesca, G. Valenti,
603 Hydraulic behaviour of calcium sulfoaluminate cement alone and in mixture with Portland
604 cement, Proc. 13th Int. Congr. Chem. Cem. Madrid (2011).

605 [28] M.D. Cohen, C.W. Richards, Effects of particle sizes of expansive clinker on strength-
606 expansion characteristics of Type K expansive, Cem. Concr. Res. 12 (1982) 717-725.

607 [29] I. Odler, J. Colan-Subauste, Investigations on cement expansion associated with ettringite
608 formation, Cem. Concr. Res. 29 (1999) 731-735.

609 [30] ACI 223-R, Guide for the Use of Shrinkage-Compensating Concrete, American Concrete
610 Institute, Farmington Hills, MI, 2010, 5 pp.

611 [31] R. Trauchessec, J. –M. Mechling, A. Lecomte, A. Roux, B. Le Rolland, Hydration of
612 ordinary Portland cement and calcium sulfoaluminate cement blends, Cem. Concr. Res. 56
613 (2015) 106-114.

614 [32] G. Le Saoût, B. Lothenbach, A. Hori, T. Higuchi, F. Winnefeld, Hydration of Portland
615 cement with additions of calcium sulfoaluminates, Cem. Concr. Res. 43 (2013) 81-94.

616 [33] M. García-Maté, A.G. De la Torre, L. León-Reina, M.A.G. Aranda, I. Santacruz,
617 Hydration studies of calcium sulfoaluminate cements blended with fly ash, Cem. Concr. Res. 54
618 (2013) 12-20.

619 [34] V. Živica, Properties of blended sulfoaluminate belite cement, Constr. Build. Mater. 14
620 (2000) 433-437.

621 [35] S. Ioannou, K. Paine, L. Reig, K. Quillin, Performance characteristics of concrete based
622 on a ternary calcium sulfoaluminate-anhydrite-fly ash cement, Cem. Concr. Comp. 55 (2015)
623 196-204.

624 [36] C. Lobo, M. Cohen, Hydration of type K expansive cement paste and the effect of silica
625 fume: I. Expansion and solid phase analysis, Cem. Concr. Res. 22 (1992) 961-969.

626 [37] K.J. Folliard, M. Ohta, E. Rathje, P. Collins, Influence of mineral admixtures on
627 expansive cement mortars, Cem. Concr. Res. 24 (1994) 424-432.

628 [38] B. Mather, "A Discussion of the Paper "Theories of Expansion in Sulfoaluminate-Type
629 Expansive Cements: Schools of Thought," by M.D. Cohen, Cem. Conr. Res. 14 (1984) 603-609.

630 [39] L. Zhang, G. W. Scherer, Comparison of methods for arresting hydration of cement,
631 Cem. Concr. Res. 41 (2011) 1024–1036.

632 [40] H. Rietveld, A profile refinement method for nuclear and magnetic structures, Journal of
633 applied Crystallography. 2 (1969) 65-71.

634 [41] A. De La Torre, S. Bruque, M. Aranda, Rietveld quantitative amorphous content analysis,
635 J. Appl. Crystallogr. 34 (2001) 196-202.

636 [42] R. Barneyback Jr., S. Diamond, Expression and analysis of pore fluids from hardened
637 cement pastes and mortars, Cem. Concr. Res. 11 (1981) 279-285.

638 [43] T. Chappex, K. Scrivener, Alkali fixation of C–S–H in blended cement pastes and its
639 relation to alkali silica reaction, Cem. Concr. Res. 42 (2012) 1049-1054.

640 [44] B. Lothenbach, Thermodynamic equilibrium calculations in cementitious systems, Mater.
641 Struct. 43 (2010) 1413-1433.

642 [45] D. Rothstein, J.J. Thomas, B.J. Christensen, H.M. Jennings, Solubility behavior of Ca-,
643 S-, Al-, and Si-bearing solid phases in Portland cement pore solutions as a function of hydration
644 time, Cem. Concr. Res. 32 (2002) 1663-1671.

645 [46] D. Damidot, B. Lothenbach, D. Herfort, F. Glasser, Thermodynamics and cement
646 science, Cem. Concr. Res. 41 (2011) 679-695.

647 [47] R.B. Perkins, C.D. Palmer, Solubility of ettringite ($Ca_6[Al(OH)_6]_2(SO_4)_3 \cdot 26H_2O$) at 5–
648 75°C, Geochim. Cosmochim. Acta. 63 (1999) 1969-1980.

649 [48] C.J. Warren, E.J. Reardon, "The solubility of ettringite at 25°C," Cem. Concr. Res. 24
650 (1994) 1515-1524.

651 [49] D. K. Nordstrom, J. L. Munoz, Geochemical Thermodynamics, Blackwell, Boston, 1988.

652 [50] T. Wagner, D. A. Kulik, F. F. Hingerl and S. V. Dmytrieva, "GEM-Selektor geochemical
653 modeling package: TSolMod library and data interface for multicomponent phase models," The
654 Canadian Mineralogist, 50 (2012) 1173-1195.

655 [51] D. A. Kulik, T. Wagner, S. V. Dmytrieva, G. Kosakowski, F. F. Hingerl, K. V.
656 Chudnenko and U. R. Berner, "GEM-Selektor geochemical modeling package: revised algorithm
657 and GEMS3K numerical kernel for coupled simulation codes," Comp. Geosci. 17 (2013) 1-24.

658 [52] T. Matschei, B. Lothenbach and F. P. Glasser, 'Thermodynamic properties of Portland
659 cement hydrates in the system $CaO–Al_2O_3SiO_2–CaSO_4–CaCO_3–H_2O$," Cem. Concr. Res. 37
660 (2007) 1379-1410.

661 [53] R. L. Day and B. K. Marsh, "Measurement of porosity in blended cement pastes," *Cem.*
662 *Concr. Res.*, 18 [1] 63-73 (1988).

663 [54] P. Chaunsali, S. Lim, P. Mondal, D. H. Tobias, D. H. Tobias, Factors Influencing the
664 Early-Age Volume Change of Expansive Cements Relevant for Bridge Deck Concrete, *Trans.*
665 *Res. Board 92nd Annual Meeting*. [13-3748] (2013).

666 [55] P. Chaunsali, P. Mondal, Influence of calcium sulfoaluminate (CSA) cement content on
667 expansion and hydration behavior of various ordinary Portland cement-CSA blends, J. Am.
668 Ceram. Soc. 1-8 (2015).

669 [56] C. Famy, K. Scrivener, A. Atkinson, A. Brough, Influence of the storage conditions on
670 the dimensional changes of heat-cured mortars, Cem. Concr. Res. 31 (2001) 795-803.

671 [57] W. Kunther, B. Lothenbach, K.L. Scrivener, On the relevance of volume increase for the
672 length changes of mortar bars in sulfate solutions, Cem. Concr. Res. 46 (2013) 23-29.

673 [58] P. Chaunsali, P. Mondal, Influence of Mineral Admixtures on Early-age Behavior of
674 Calcium Sulfoaluminate Cement, *ACI Mat. J.* 112 (2015) 59-68.

675 [59] M. Andac, F. Glasser, Pore solution composition of calcium sulfoaluminate cement, Adv.
676 Cem. Res. 11 (1999) 23-26.

677 [60] F. Winnefeld, B. Lothenbach, Hydration of Calcium Sulfoaluminate Cements -
678 Experimental Findings and Thermodynamic Modelling, Cem. Concr. Res. 40 (2010) 1239-1247.

679 [61] H.F. Taylor, Cement Chemistry, Thomas Telford, 1997.

680 [62] M. H. Shehata, M.D.A. Thomas, R. F. Bleszynski, The effects of fly ash composition on
681 the chemistry of pore solution in hydrated cement pastes, Cem. Concr. Res. 29 (1999) 1915-
682 1920.

683 [63] J. Bizzozero, C. Gosselin, K.L. Scrivener, Expansion mechanisms in calcium aluminate
684 and sulfoaluminate systems with calcium sulfate, Cem. Concr. Res. 56 (2014) 190-202.

685 [64] S. Timoshenko, J. Goodier, Theory of elasticity, 3rd Ed. McGraw-Hill, New York, 1970.

686 [65] O. Coussy, Deformation and stress from in-pore drying-induced crystallization of salt, J.
687 Mech. Phys. Solid. 54 (2006) 1517-1547.

688 [66] S. Ghabezloo, J. Sulem, S. Guédon, F. Martineau, J. Saint-Marc, Poromechanical
689 behaviour of hardened cement paste under isotropic loading. Cem. Concr. Res. 38(2008) 1424-
690 1437.

691 [67] R.M. Espinosa-Marzal, A. Hamilton, M. McNall, K. Whitaker, G. W. Scherer, The
692 chemomechanics of crystallization during rewetting of limestone impregnated with sodium
693 sulfate, J. Mater. Res. 26 (2011) 1472-1481.

694 [68] R. J. Flatt, F. Caruso, A. M. A. Sanchez and G. W. Scherer, "Chemo-mechanics of salt
695 damage in stone," Nat. Comm. 5 (2014).

696 [69] M. Balonis, F. P. Glasser, The density of cement phases, Cem. Concr. Res. 39 (2009)
697 733-739.

[70] M. Steiger, Crystal growth in porous materials—I: The crystallization pressure of large crystals, J. Cryst. Growth. 282 (2005) 455-469.

[71] J. K. Mackenzie, The elastic constants of a solid containing spherical holes, Proc. Phy. Soc. B 63 (1950).

[72] Z. C. Grasley, G. W. Scherer, D. A. Lange, J. J. Valenza, Dynamic pressurization method of measuring permeability and modulus: II. cementitious materials, Mater. Struct. 40 (2007) 711-721.

[73] S. A. Altoubat, D.A. Lange, Creep, shrinkage, and cracking of restrained concrete at early age, ACI Mater. J. 98 (2001) 323-331.